Simulation of Binary Mixture Adsorption of Methane and CO_2 at Supercritical Conditions in Carbons

Yohanes Kurniawan, Suresh K. Bhatia, and Victor Rudolph
Division of Chemical Engineering, The University of Queensland, Brisbane, QLD 4072, Australia

DOI 10.1002/aic.10687
Published online October 7, 2005 in Wiley InterScience (www.interscience.wiley.com).

Knowledge of the adsorption behavior of coal-bed gases, mainly under supercritical high-pressure conditions, is important for optimum design of production processes to recover coal-bed methane and to sequester CO_2 in coal-beds. Here, we compare the two most rigorous adsorption methods based on the statistical mechanics approach, which are Density Functional Theory (DFT) and Grand Canonical Monte Carlo (GCMC) simulation, for single and binary mixtures of methane and carbon dioxide in slit-shaped pores ranging from around 0.75 to 7.5 nm in width, for pressure up to 300 bar, and temperature range of 308-348 K, as a preliminary study for the CO_2 sequestration problem. For single component adsorption, the isotherms generated by DFT, especially for CO_2, do not match well with GCMC calculation, and simulation is subsequently pursued here to investigate the binary mixture adsorption. For binary adsorption, upon increase of pressure, the selectivity of carbon dioxide relative to methane in a binary mixture initially increases to a maximum value, and subsequently drops before attaining a constant value at pressures higher than 300 bar. While the selectivity increases with temperature in the initial pressure-sensitive region, the constant high-pressure value is also temperature independent. Optimum selectivity at any temperature is attained at a pressure of 90-100 bar at low bulk mole fraction of CO_2, decreasing to approximately 35 bar at high bulk mole fractions. *AIChE J,* 52: 957–967, 2006
Keywords: adsorption, binary mixture, CO_2 sequestration, density functional theory, simulation

Introduction

Climate change associated with the rapid buildup of greenhouse gases (GHG), such as carbon dioxide, methane, and NO_x, in the atmosphere is now generally accepted as a serious worldwide concern. Carbon dioxide emissions present the main problem, since they account for about 60% of the human induced global warming load.[1] One of the responses for reducing CO_2 emissions is to capture them at large industrial sources and then store them in the earth rather than discharging them to the atmosphere. A range of technologies under the broad title of Carbon Capture and Storage (CCS) have been proposed for achieving this.

One of the most prospective methods for sequestering CO_2 in the earth is by injecting it into coalbed methane (CBM) reservoirs. The CO_2 displaces methane from the seam and is itself permanently trapped and held within the coal.

Enhanced CBM processes use injection gases in order to improve methane recovery from the reservoir (by up to 50%) and increase the production rate per producing well. The nature of the injection gas depends on commercial considerations, but could be flue gas (a mixture of mainly N_2 and CO_2), or partially or fully CO_2 enriched flue gas. The main benefit of CO_2-ECBM is through gaining the dual advantages of improved methane recovery together with CO_2 disposal.

The implementation of ECBM requires knowledge of the

Correspondence concerning this article should be addressed to S. K. Bhatia at sureshb@cheque.uq.edu.au.

sorption characteristics, on particular coals at appropriate underground conditions, of the main gases and their mixtures. This also underlies any simulation work to determine CBM production rate, storage capacity, displacement interactions, operating conditions, and economic feasibility.[2]

This article focuses on high-pressure single and binary gas sorption equilibrium of CO_2 and CH_4 in an idealized slit pore system, commonly used for modeling adsorption in carbons. The pore walls are assumed infinitely thick and comprised of stacked graphene sheets. The conditions that are considered are otherwise reasonable for deep coal CBM reservoirs[3] and include: temperatures of 308 K, 318 K, 338 K, and 348 K; pressures up to 100 bar; and micropore widths (H) in the range of 0.7–7.5 nm.

We compare high-pressure sorption equilibria using two different approaches, namely, Density Functional Theory (DFT) and the Monte Carlo simulation method in the grand canonical ensemble (GCMC). The latter has been used as a benchmark to evaluate other methods and for determining the accuracy of the approximate free energy density functional in DFT. Both methods have previously been successfully applied to model sorption of supercritical gases, such as Ar, CH_4, and CO_2, with simple molecular structures.[4-11]

Theoretical Modeling

Density Functional Theory

The Density Functional Theory (DFT) is based on a mean field approximation of the fluid-fluid interaction. It provides a good description of a simple confined fluid and also has the advantage of being computationally less demanding than the full Monte Carlo simulation. In DFT, two central quantities, treated as unique functionals of the density distribution $\rho(\mathbf{r})$, are the grand potential $\Omega[\rho]$ and the intrinsic Helmholtz free energy $F[\rho]$ (i.e., the Helmholtz energy in the absence of the external field), which are related according to

$$\Omega[\rho] = F[\rho] + \int d\mathbf{r}\rho(\mathbf{r})[u(\mathbf{r}) - \mu] \tag{1}$$

in which μ is the chemical potential and u(r) is the external potential experienced by the adsorbate molecules due to the pore walls. The $F[\rho]$ itself contains two contributions

$$F[\rho] = F_{id}[\rho] + F_{ex}[\rho] \tag{2}$$

The ideal gas contribution $F_{id}[\rho]$ is the free energy of the system with the same density but without internal interactions among the particles, and is given by the exact relation

$$\beta F_{id}[\rho] = \int d\mathbf{r}\rho(\mathbf{r})\{\ln[\rho(\mathbf{r})\lambda^3] - 1\} \tag{3}$$

where $\beta = 1/k_BT$ is the inverse temperature, k_B is the Boltzmann's constant, and $\lambda = h(2\pi mk_BT)^{-1/2}$ is the thermal de Broglie wavelength.

The other contribution, $F_{ex}[\rho]$, which is generally unknown, is the excess free energy distribution caused by interparticle interactions and is approximated by introducing perturbation theory. According to perturbation theory, the pair interaction can be divided into a repulsive and an attractive part, following

$$u(\mathbf{r}) = u_{\text{rep}}(\mathbf{r}) + u_{\text{att}}(\mathbf{r}) \tag{4}$$

The excess free-energy functional $F_{\text{ex}}[\rho]$ for the model system can be approximated as the sum of the repulsive and attractive contributions $F_{\text{rep}}[\rho]$ and $F_{\text{att}}[\rho]$, respectively, i.e.,

$$F_{\text{ex}}[\rho] = F_{\text{rep}}[\rho] + F_{\text{att}}[\rho] \tag{5}$$

Under the mean field approximation, the attractive part leads to

$$F_{\text{att}}[\rho] = \frac{1}{2}\int \rho(\mathbf{r})d\mathbf{r}\int d\mathbf{r}'\rho(\mathbf{r}')\phi_{\text{att}}(|\mathbf{r} - \mathbf{r}'|) \tag{6}$$

The repulsive part is the major uncertainty, which causes differences with other versions of DFT, as the exact result for this part is unknown. Here we use the Denton and Ashcroft[12] formulation, utilized earlier by Bhatia.[13,14]

The solution for the equilibrium density distribution of an adsorbed gas in a confined pore is obtained by the minimization of the grand free energy (or grand potential), which satisfies

$$\frac{\delta\Omega[\rho]}{\delta\rho(\mathbf{r})} = 0 \tag{7}$$

leading to the Euler-Lagrange relation

$$\rho(\mathbf{r}) = z\exp\{-\beta u(\mathbf{r}) + c^{(1)}(\mathbf{r};[\rho]) - \beta\int d\mathbf{r}'\rho(\mathbf{r}')\phi_{\text{att}}(|\mathbf{r} - \mathbf{r}'|)\} \tag{8}$$

where $z = e^{\beta}\mu/\lambda^3$ (the fugacity) and $c^{(1)}(\mathbf{r};[\rho])$ denotes the one-particle direct correlation function (DCF), following

$$c^{(1)}(\mathbf{r};[\rho]) = -\beta\frac{\delta(F_{\text{ex}})}{\delta\rho(\mathbf{r})} \tag{9}$$

Equation 8 is a formally exact relation, which in principle may be solved for $\rho(\mathbf{r})$ if the functional $c^{(1)}(\mathbf{r};[\rho])$ is known. In practice, however, this functional is generally unknown and must be approximated. Here a simple version of the Weighted Density Approximation (WDA) of Denton and Ashcroft[12] was adopted to model the non-uniform hard-sphere fluid. The approximation is expressed by the simple relation

$$c^{(1)}_{\text{WDA}}(\mathbf{r};[\rho]) \equiv c_0^{(1)}(\bar{\rho}(\mathbf{r})) \tag{10}$$

which equates the one-particle DCF of a *nonuniform* fluid to its counterpact $c_0^{(1)}$ for the corresponding *uniform* fluid evaluated at the weighted density $\bar{\rho}(\mathbf{r})$. The weighted average, $\bar{\rho}(\mathbf{r})$, with respect to a weight function w, is then defined according to

$$\bar{\rho}(\mathbf{r}) \equiv \int d\mathbf{r}'\rho(\mathbf{r}')w(|\mathbf{r}-\mathbf{r}'|;\bar{\rho}(\mathbf{r})) \tag{11}$$

where the expressions for the weight function and $c_0^{(1)}(\rho)$ are provided elsewhere.[12,13]

The Lennard-Jones 12–6 pair potential is used to model the interactions among adsorbate molecules. The attractive interactions are modeled using the Weeks-Chandler-Anderson (WCA) perturbation scheme[15]:

$$\phi_{\text{att}}(r) = \begin{cases} -\varepsilon_{ff}, & r < r_m \\ \phi_{ff}, & r_m < r < r_c \\ 0, & r > r_c \end{cases} \tag{12}$$

where ε_{ff} is the potential well depth, $r_{\text{m}} = 2^{1/6}\sigma_{ff}$ is the separation at the minimum of the potential, and r_{c} is the cutoff distance.

Grand Canonical Monte Carlo simulation

The Monte Carlo method is originally a mathematical and numerical technique invented to solve complex stochastic problems that are inaccessible to rigorous analytical methods. Here, this technique is carried out in the grand canonical ensemble, including moves for translation or reorientation, creation, and destruction of particles in the simulation box, with successive trials based on a Markov chain. A decision is made according to the Metropolis sampling scheme[16,17] whether to accept each trial or return to the old configuration based on a prescribed probability for each trial move. While the number of particles and associated configurational energy are randomly changed to generate a new configuration, micropore volume, temperature and adsorbate chemical potential are fixed, corresponding to the experimental condition in which the adsorbed molecule is in equilibrium with a bulk gas. Therefore, this method is now standard and has been frequently described elsewhere.[16,18] In our implementation, the fluid-fluid interaction potential is modeled using a Lennard-Jones potential truncated at 1.5 nm. The solid-fluid interaction potential is represented by the Steele 10–4-3 potential.[19] The size of the simulation box, which is always greater than twice the cutoff distance, and the number of configurations/trials to obtain an equilibrium condition are set to $16.5\sigma_{\text{ff}}$ and 3×10^6, respectively. Typical calculations for a single point require between 35 and 45 minutes of CPU time on a Pentium 4.

Adsorbent model

The microporous surface was approximated by a homogeneous potential function as an assembly of close-packed atoms, each of which is characterized by the potential parameters ε and σ. In the slit pore model[20-26] used, the pore comprises two parallel graphitic slabs. The distance between the center of the carbon atoms on each opposing slab is defined as the physical pore width, H_{phys}. The influence of connectivity in the pore was neglected by the assumption that the ratio of pore length to pore width is large.

Potential models

Here we use the one-center potential model for either methane or carbon dioxide to simplify the simulation process. For carbon dioxide, the alternate more representative 3-center model is known to be more accurate at saturation conditions,[27] attained at very high pressures of about 3000 bar. However, at low and moderate densities, the single-center model is adequate.[28]

The intermolecular interaction potential energy between two fluid molecules is assumed to be governed by the 12–6 Lennard-Jones model:

$$\phi_{ff} = 4\varepsilon_{ff}\left[\left(\frac{\sigma_{ff}}{r_{ij}}\right)^{12} - \left(\frac{\sigma_{ff}}{r_{ij}}\right)^{6}\right] \tag{13}$$

where r is the separation distance between two fluid atoms. ε_{ff} and σ_{ff} are fitted parameters for the bulk adsorbate well depth and molecular diameter, respectively. This potential energy is in a good agreement in the description of noble gases and many spherical molecules (such as methane) in the homogeneous bulk phase.

We model the wall as an infinitely thick graphite slab. Two parallel surfaces separated by a distance H between centers of surface carbon atoms constitute a model slit-shaped pore. Assuming the Lennard-Jones pairwise interaction potential, Steele[19] has described the interaction potential for this single graphite slab and a single fluid molecule by:

$$\phi_{sf} = A\left[\frac{2}{5}\left(\frac{\sigma_{sf}}{z}\right)^{10} - \left(\frac{\sigma_{sf}}{z}\right)^{4} - \frac{\sigma_{sf}^4}{3\Delta(0.61\Delta + z)^3}\right] \tag{14}$$

where A is $2\pi\sigma_{sf}^2\varepsilon_{sf}\rho_s\Delta$, z is the distance of the fluid particle from the graphite surface, σ_{sf} is the effective adsorbate-adsorbent (carbon) intermolecular diameter, Δ is the separation between graphite layers (0.335 nm), ρ_s is the number of carbon atoms per unit volume in graphite (114 nm^{-3}), and ε_{sf} is the parameter for the adsorptive-graphite interaction potential well-depth. The solid-fluid parameters were calculated by combining the graphite parameters with the appropriate fluid parameters using the Lorentz-Berthelot mixing rules[16]:

$$\varepsilon_{sf} = \sqrt{\varepsilon_{ss}\varepsilon_{ff}}$$

$$\sigma_{sf} = \frac{\sigma_{ss} + \sigma_{ff}}{2} \tag{15}$$

The Steele potential describes the interactions between the adsorbate molecule and one side of the graphite wall; however, in slit-pore geometry, the adsorbate molecule will interact with both pore walls, and hence the wall potential within the pore for the slit system of physical width H is given as:

$$\Phi = \phi_{sf}(H - z) + \phi_{sf}(z) \tag{16}$$

This equation ignores the surface corrugation, which is unlikely to significantly affect the results at high enough temperatures.[29]

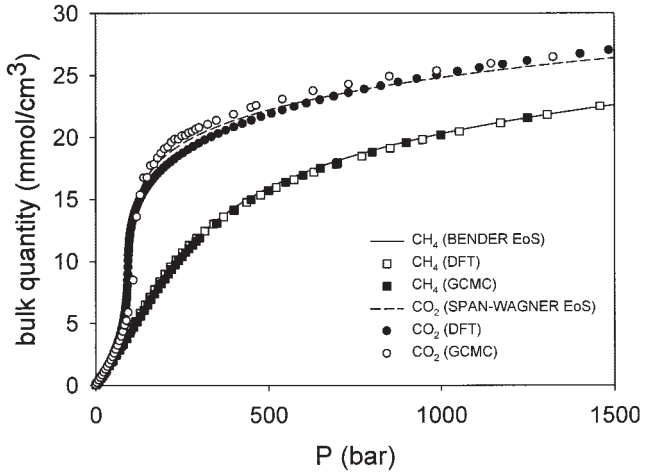

Figure 1. Bulk isotherm of methane and carbon dioxide at 318.15 K.

Results and Discussion

Parameter estimation

Initially, bulk isotherms were fitted for both CH_4 and CO_2 to determine suitable L-J parameters using each method. Fitting of bulk fluid data to obtain L-J parameters depends upon the range of adsorbed densities or pressures involved. For this case, it is desired to simulate or calculate isotherms by the DFT and GCMC methods, for adsorption in a slit-pore up to 100 bar, for which the density of the adsorbed phase at that pressure approaches approximately 20 mmol/cm^3. Therefore, it is necessary to fit the density from bulk simulation or DFT calculation to bulk experimental data up to this density. Here we represent the experimental data by using an appropriate equation of state, up to this density (20 mmol/cm^3), which is attained at about 1500 bar.

Fluid-fluid interaction, either for carbon dioxide or for methane, is modeled by the Lennard-Jones equation, as discussed earlier. Values of ε_{ff} and σ_{ff} for methane and carbon dioxide were obtained by fitting either the DFT or GCMC predictions to the bulk thermodynamic data up to 1500 bar that were estimated from a suitable equation of state at 318.15 K. We used the Bender[30] and Span-Wagner equations of state,[31] which are the current standard for methane and carbon dioxide, respectively, and both of them are accepted as essentially equivalent to experimental data. The quality of fitting, which can be seen in Figure 1, is much better in the case of methane. From the fluid-fluid interaction parameters, we can determine the solid-fluid interaction parameters by adopting the standard Lorentz-Berthelot (LB) mixing rules, the composite parameter σ_{sf} being the arithmetic mean of the gas and carbon values, and the composite parameter ε_{sf} being the geometric mean. We used the following parameters for the carbon surface: σ_{ss} = 3.4 Å, ε_{ss}/k = 28 K.[19] All parameter values used in the calculations are listed in Table 1. It should be noted here that the LB mixing rules are only an approximation, and not necessarily accurate in general. More accurate rules involve additional binary interaction parameters[32] that would need to be fitted to data, and for the present simulation study the simple LB prescription suffices.

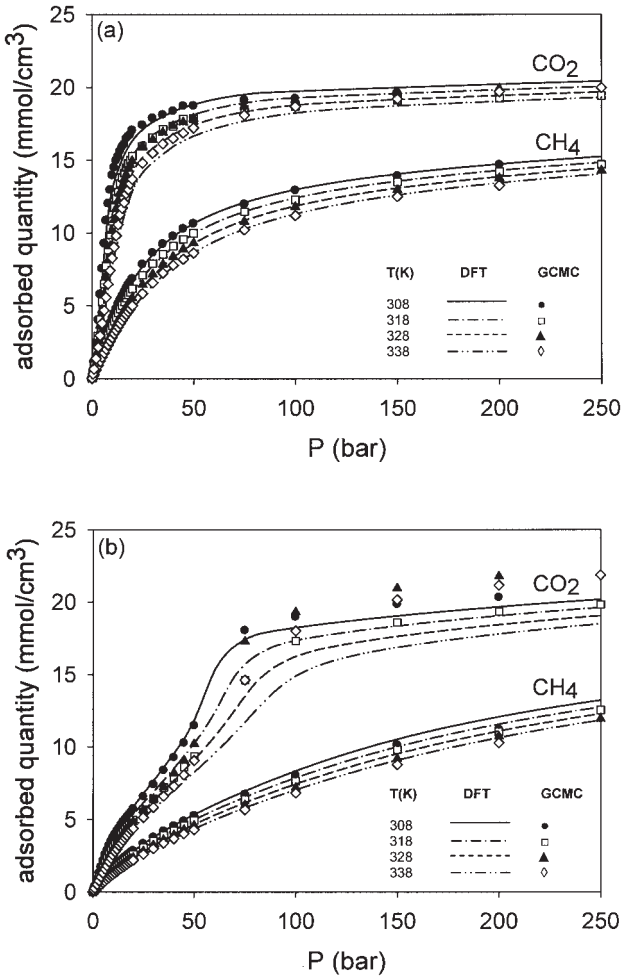

Figure 2. Comparison between DFT calculated and GCMC simulated adsorption isotherms of supercritical methane and carbon dioxide at reduced slit-width (*H) equal to (a) 4 and (b) 10, for four different temperatures.**

Single component adsorption

Absolute adsorption isotherms have been calculated as depicted in Figures 2a and b for several temperatures at two

Table 1. Parameters Used for the Calculation of Model Isotherms

	DFT				GCMC			
Adsorptive	ε_{ff}/k_B (K)	σ_{ff} (Å)	ε_{sf}/k_B (K)	σ_{sf} (Å)	ε_{ff}/k_B (K)	σ_{ff} (Å)	ε_{sf}/k_B (K)	σ_{sf} (Å)
CH_4	137.9353	3.651206	62.1465	3.5256	148.0	3.751	64.3739	3.5755
CO_2	223.0192	3.502010	79.0224	3.4510	242.0	3.615	82.3165	3.5075

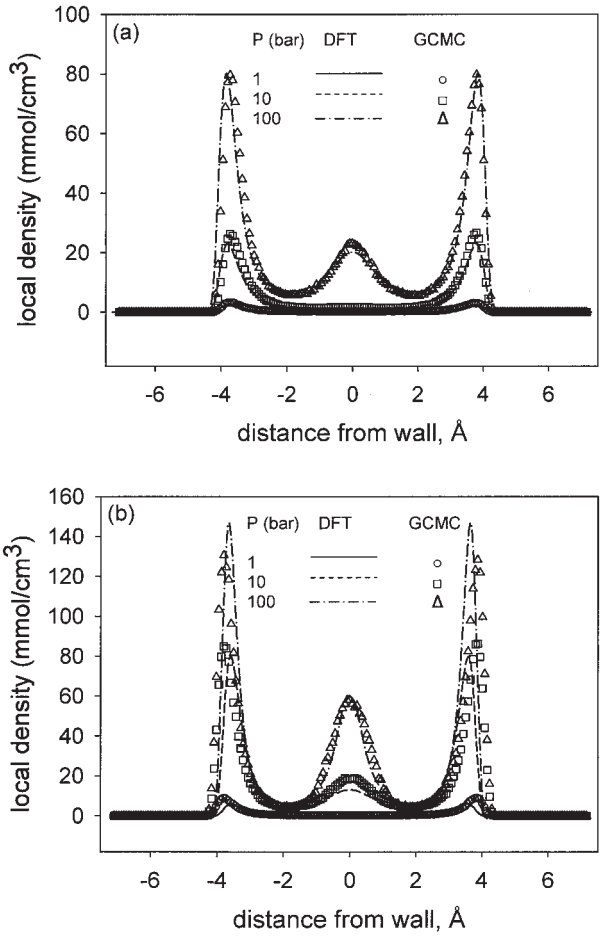

Figure 3. Comparison between DFT calculated and GCMC simulated local density profile at 318 K and reduced slit-width (*H) equal to 4, for (a) methane and (b) carbon dioxide, for three different pressures.**

different reduced slit-widths, for pure methane and carbon dioxide adsorbed by slit-like pores in model graphite using the parameters of Table 1. Here the reduced slit-width is given by $H^* = H/\sigma_{CH_4}$. From both figures, it is seen that carbon dioxide adsorbs more than methane over the entire temperature range as a result of stronger interaction. The latter will be discussed subsequently. While the amount adsorbed for methane from DFT results matches very well with GCMC at $H^* = 4$, there is some deviation for carbon dioxide. At the larger pore size $H^* = 10$, both gases show deviation in the results between DFT and GCMC at pressure over 50 bar, in which CO_2 again gives a bigger deviation. This may be caused by the different quality of fit of DFT and GCMC to bulk isotherm for CO_2, which is evident in Figure 1, and also the approximate nature of the DFT method used.[12]

To investigate the effect of pressure and the effect of pore size on the layering mechanism of molecules, we show the local density profiles for both pure CH_4 and CO_2 in Figures 3 and 4. Figures 3a and 3b show the local density distribution of methane and carbon dioxide, respectively, versus distance across the pore having reduced slit-width (H^*) of 4. The three distributions in these figures correspond to the bulk pressures of 1, 10, and 100 bar at adsorption temperature of 318 K. The figure shows good agreement between DFT and GCMC for methane, except for high pressure at the center of the wall, where the GCMC prediction is slightly larger than DFT results. Further, none of the pressure conditions give similar agreement between these two methods for carbon dioxide. Moreover, at the same pressure of 100 bar, we can see from Figure 4a that the GCMC result is also slightly higher in the small reduced pore size ($H^* = 2$) for methane.

Contrary to methane, GCMC results for carbon dioxide are always slightly higher for $H^* \geq 2$, as can be seen in Figure 4b. To this extent, we will not use the DFT model in our subsequent calculation because of its prediction inadequacy in the present case. This is most likely because the temperature is close to the critical point of CO_2, in which case mean field theory can be inadequate. From Figures 3 and 4, we observe oscillation in the density distribution, suggesting a layering mechanism for adsorption of the gas. The density approaches its maximum values in the proximity of the pore walls, where the solid-fluid potential energy is minimum (as seen in Figure

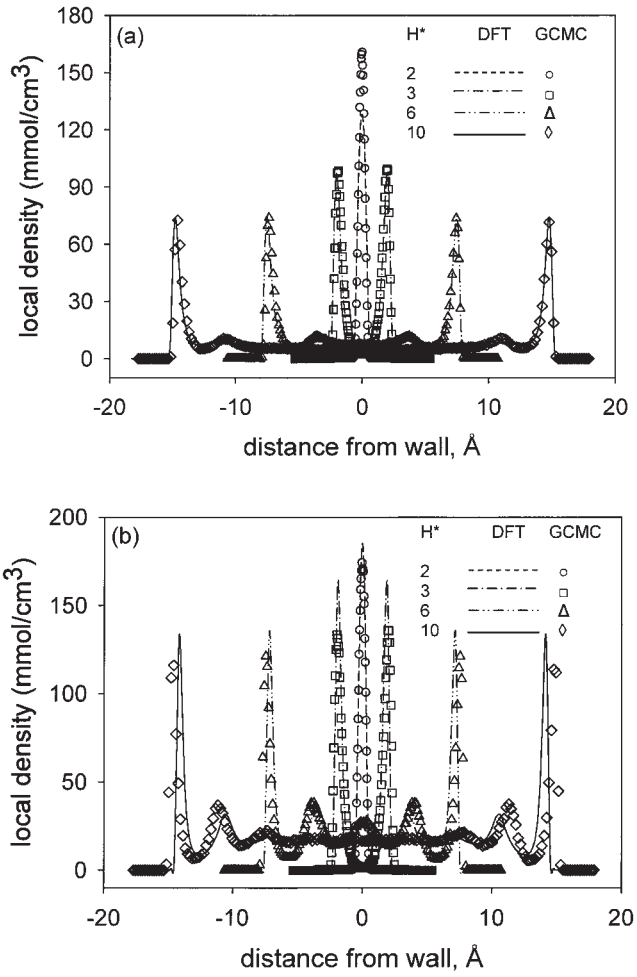

Figure 4. Comparison between DFT calculated and GCMC simulated local density profile at 318 K and 100 bar, for (a) methane and (b) carbon dioxide, for four different reduced slit-widths (*H)**

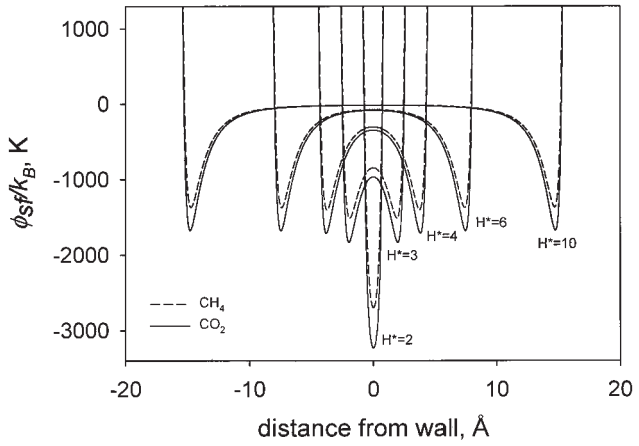

Figure 5. Solid-fluid interaction potential for methane and carbon dioxide in pores of reduced slit-width H^* = 2- 10, at temperature 318.15 K.

5), resulting in the formation of relatively thin and dense layers close to the surfaces of each wall. Each of these layers exerts its own potential field, with the minimum occurring at a distance of roughly one collision diameter. This is the reason for the appearance of the second and higher molecular layers. Additionally, the thermal motion and relatively weak fluid-fluid molecular interaction results in low intensity of the second peak and even much lower intensity of the third peak from the wall. Therefore, only two peaks are clearly distinguished in the distribution for high pore-size.

Figure 5 shows the gas-solid potential profile of methane and carbon dioxide in graphite slit pores of different widths. This potential is shown as a function of the distance z from the wall only, which is calculated as the sum of the interactions from both walls using Eq. 16. For each case, the gas-solid potential is calculated using the 10–4-3 potential to represent the interaction between the molecule and the graphite slabs that bound the slit pore. It can be seen from the Figure that the interaction potential between carbon dioxide and the pore is significantly more attractive than between methane and the pore (solid-fluid potentials substantially below zero), and the potential becomes deeper with decreasing reduced pore-width (H^*). The double minima merge to produce a single minimum for $H^* = 2$, and the potential at the central position is significantly lowered by the overlapping. In the center, the potential depth of carbon dioxide is about twice deeper than that of methane for $H^* = 2$, while in other slit widths it is deeper by a factor of around 1.14 in all cases. This stronger interaction potential is responsible for the larger adsorption of CO_2 seen in Figure 2.

Adsorption of CH_4-CO_2 mixtures

There is a general expectation that CO_2 is preferentially adsorbed from CH_4/CO_2 mixtures under competitive sorption conditions. When the system consists of adsorbates with different molecular properties, the difference in interaction energies will lead to enhancement of one adsorbate relative to the others (selectivity). The equilibrium selectivity of carbon dioxide with respect to methane is defined as[33]:

$$S_{CO_2/CH_4} = \frac{x_{CO_2}/x_{CH_4}}{y_{CO_2}/y_{CH_4}} \tag{17}$$

representing the ratio of the mole fractions of the two species in the pore relative to the ratio of the mole fractions in the bulk. Values greater than unity imply that carbon dioxide is preferentially adsorbed compared to methane; in contrast, if the selectivity is smaller than unity, methane is preferentially adsorbed.

GCMC simulations have been conducted here for the adsorption of CH_4/CO_2 mixtures, and in further discussion the DFT has not been utilized because of its inaccuracy, as discussed above. The variation of selectivity with pressure for various temperatures at pore width $4\sigma_{CH_4}$ and $y_{CO_2} = 0.5$ (here y_{CO_2} is the bulk CO_2 mole fraction) can be seen in Figure 6a. It shows that selectivity initially increases with pressure to a maximum value at about 40-50 bar for every temperature and then reduces with increasing pressure. Initially, as the pressure is increased, more CO_2 is adsorbed. Subsequently, CO_2 is saturated in the pore while CH_4 adsorbs further. At high pressure, CO_2 is already adsorbed at close to the maximum density

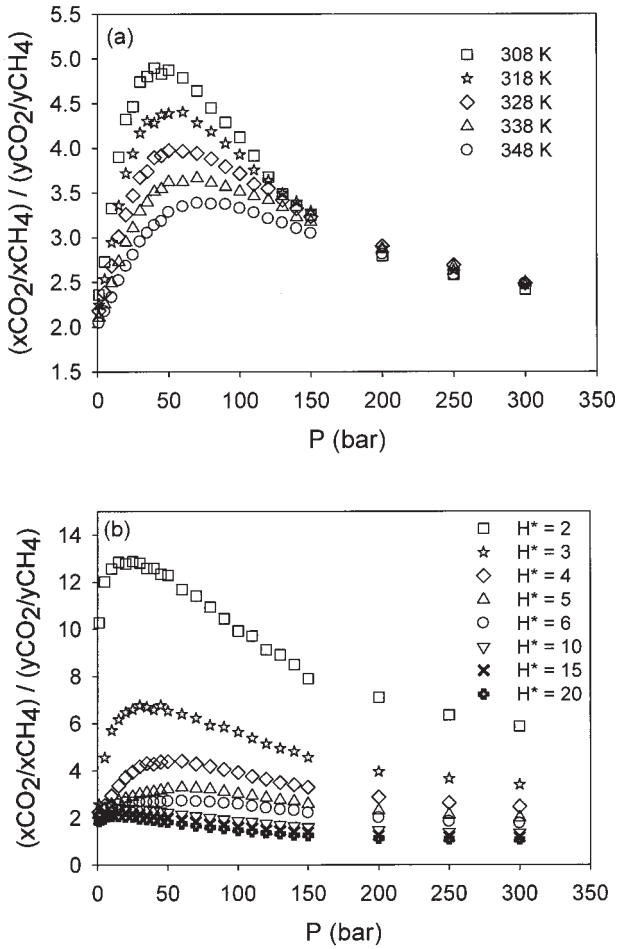

Figure 6. Selectivity of CO_2 relative to CH_4 vs. pressure.

(a) In pores of reduced slit-width $H^* = 4$ at five different temperatures; (b) in pores of various reduced slit-widths at 318 K. The gases have equal bulk mole fractions, i.e. $y_{CO_2} = 0.5$

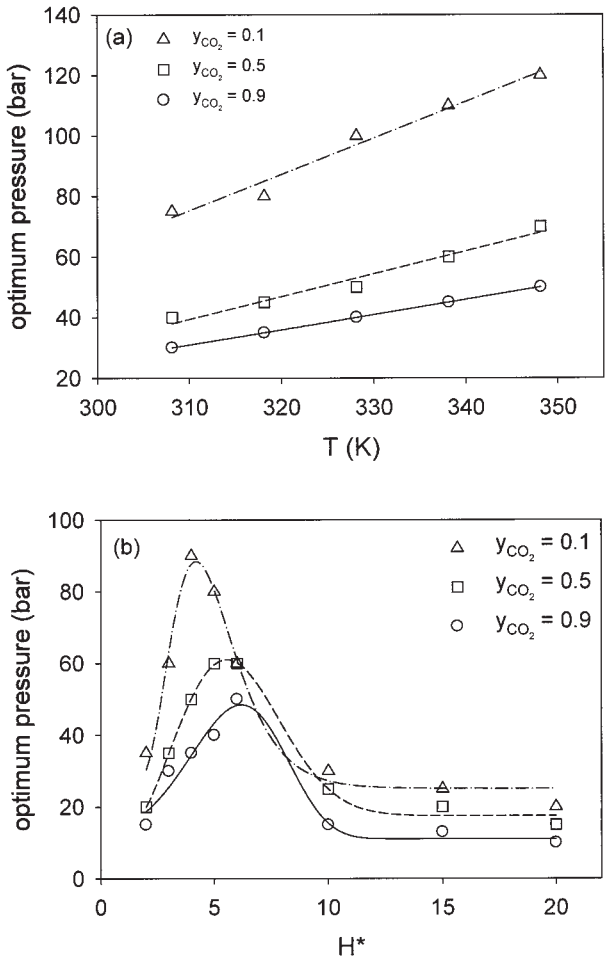

Figure 7. Variation of optimum pressure for maximum selectivity at three different bulk mole fractions of CO_2:

(a) With temperature, at $H^* = 4$; (b) with pore size, at 318 K. The lines are drawn to guide the eye.

in the pore. However, density of CH_4 keeps increasing with pressure because the critical temperature of CO_2 (304.12 K) is very high compared with the critical temperature of CH_4 (190.56 K). Thus, as we increase the pressure, methane is increasingly compressed more at high pressure. The rise of density of methane in the pore causes the selectivity to come down and ultimately appear to become independent of pressure. At a temperature of 318 K, the selectivity value is higher in the smaller pore-sizes, as shown in Figure 6b, as the smaller pore-sizes give stronger solid-fluid potential interaction (cf. Figure 5). Both graphs (Figure 6a and 6b) would suggest that selectivity is not very sensitive to pressure above about 300 bar, although further simulations at higher pressures are needed to confirm this. Such high pressures are, however, not pertinent to sequestration, and therefore not examined here.

From Figure 6, we obtain an optimum pressure, which gives maximum selectivity, for certain conditions (particular temperature and pore size). These results are depicted in Figure 7, showing the variation of optimum pressure with temperature and pore size. It is seen that in order to obtain maximum selectivity, it is necessary to increase the pressure for lower CO_2 in the bulk; that is, optimum pressure for lower y_{CO_2} is always higher than higher y_{CO_2} in the bulk for all temperatures in the range studied. We also observed that the optimum pressure increases linearly with increase in mole fraction of CO_2 in the bulk. In the real CBM reservoir condition, the bulk composition varies during production and cannot be specified uniquely. Therefore, it is necessary to determine pressure and temperature conditions that can give maximum selectivity over a range of bulk compositions. As in Figure 7a, in Figure 7b we find that the optimum pressure for lower y_{CO_2} is always higher than that at higher y_{CO_2} in the bulk for all ranges of pore size. However, in the region of y_{CO_2} lying between 0.5 and 0.9, the optimum pressure changes only slightly, and a value of about 35 bar may be a reasonable compromise given that micropores in carbons are typically 1 nm or smaller in width.

Figure 8a shows the selectivity CO_2/CH_4 as a function of y_{CO_2} at five bulk pressures in the range of 1-200 bar. At 1 bar, the selectivity is nearly constant with bulk mole fraction of carbon dioxide, while at 10 and 50 bar the selectivity increases monotonically. At a pressure of 50 bar and $y_{CO_2} = 0.8$, the

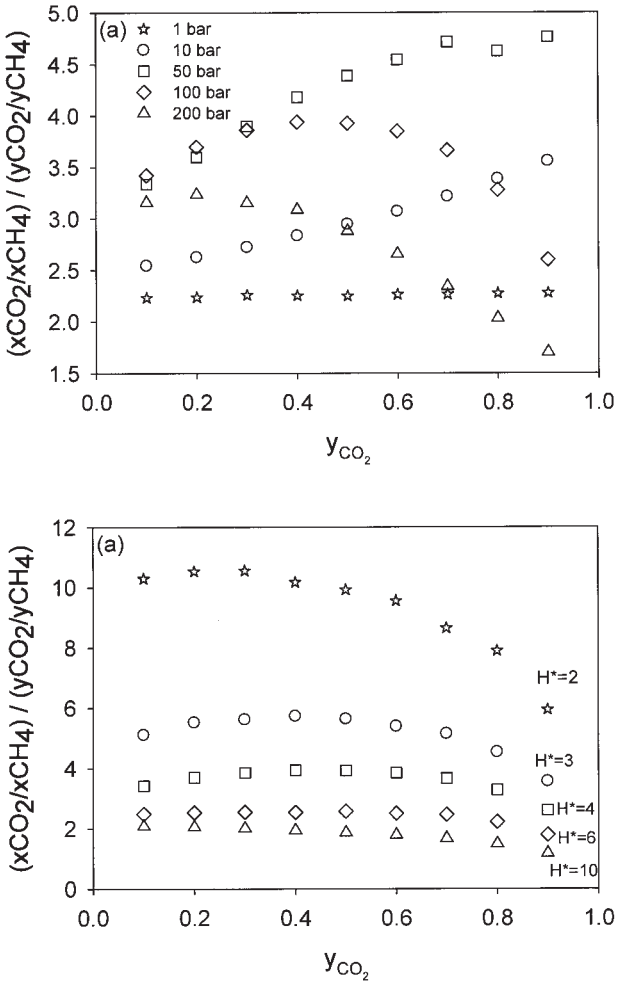

Figure 8. Selectivity of CO_2 over CH_4 as a function of bulk mole fraction of CO_2:

(a) At 318 K, and five different pressures for $H^* = 4$, and (b) at 318 K and 100 bar for several different reduced slit-widths (H^*).

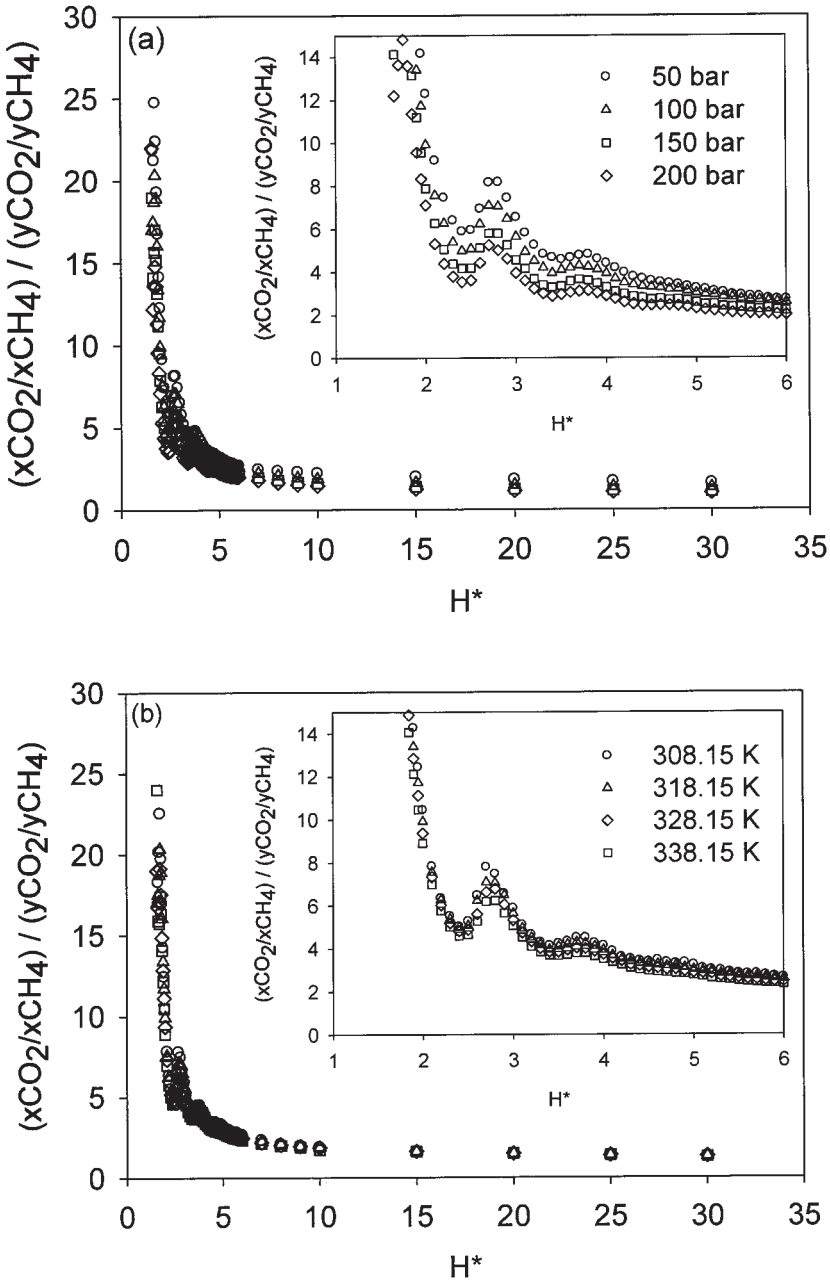

Figure 9. Selectivity of CO_2 over CH_4 as a function of reduced slit-width.

(a) At 318K and four different pressures; (b) at 100 bar and four temperatures. The gases have equal bulk mole fractions, i.e. $y_{CO_2} = 0.5$

.

selectivity becomes constant after an initial increase; however, at the higher pressures of 100 and 200 bar, it decreases after reaching a maximum. This is due to the relative saturation of the pores with CO_2 at lower y_{CO_2} when the bulk pressure is higher. Figure 8b depicts the variation of selectivity of CO_2 over CH_4 with bulk mole fraction of CO_2 for various H^*, at 318 K and pressure 100 bar. Each of the pore sizes gives a similar trend, with the selectivity increasing with bulk mole fraction of CO_2 up to y_{CO_2} equal to about 0.3-0.4, and then decreasing. As in Figure 8a, the selectivity decreases after the maximum occurs, as the CO_2 density in the pore reaches saturation. As expected, this occurs at lower y_{CO_2} at smaller pore sizes.

Figure 9 exhibits the variation of the separation factor (selectivity) with the pressure or temperature and the pore size. In all investigated pores and over the whole pressure and temperature range, the selectivity is much greater than unity, which indicates the preferential adsorption of carbon dioxide. Specifically, the relationship between selectivity and pore size at four different pressures: 50 bar, 100 bar, 150 bar, and 200 bar for the CO_2/CH_4 system is shown in Figure 9a, while the same relationship at four different temperatures (308 K, 318 K, 328 K, and 338 K) is given in Figure 9b. Figure 9a shows that selectivity is not very sensitive to pressure in larger pores, reaching almost a constant value above $H^* = 6$. As seen in

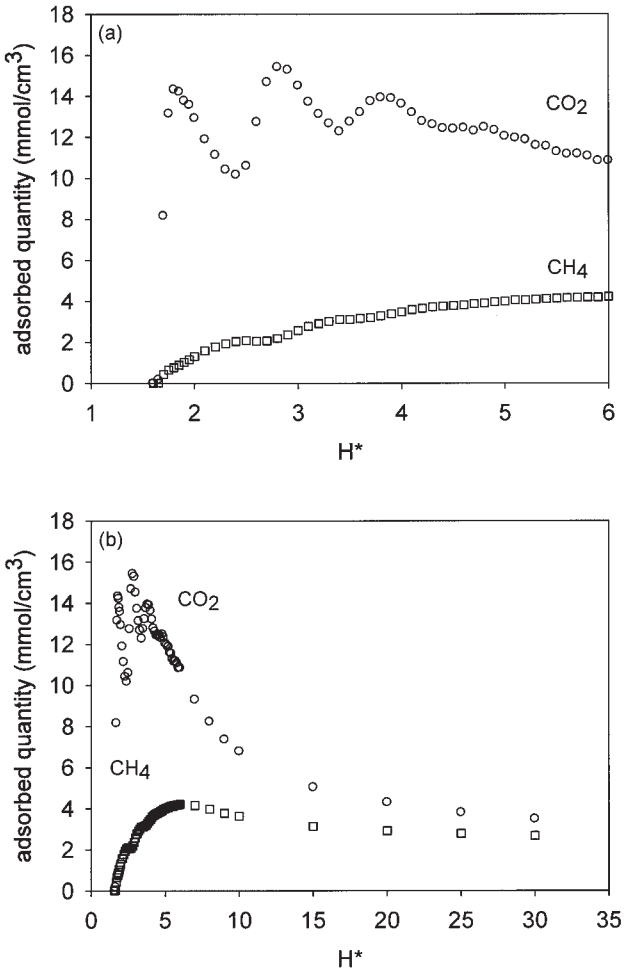

Figure 10. Adsorbed density of methane and carbon dioxide at temperature 318 K and $y_{CO_2} = 0.5$, in: (a) pores of reduced slit-width $H^* < 6$, and (b) pores of reduced slit-width $H^* < 30$.

Figure 9b, the selectivity does not change significantly with temperature, especially between 308 K and 318 K. At the limit of small pore size, the selectivity of CO_2 over CH_4 goes to infinity. This occurs because the CO_2 molecule has a slightly smaller diameter than methane (cf. Table 1) and higher ε_{ff}; it, therefore, experiences a strong attraction in pores that are repulsive to methane. This may, therefore, be considered a pore exclusion effect at small pore size. At slightly larger pore size, where both gases can enter the pore, the CH_4 density is finite, and we obtain finite selectivity. In all graphs, the selectivity in small pores is corrugated and displays two maxima (see the inset curves) before decaying with additional pressure or temperature at larger pore size. The first peak is located at a dimensionless slit width of 2.7 and the second one at a dimensionless slit width of 3.8. These extremes are located at approximately the same pore sizes as were found for the mixture of carbon dioxide and nitrogen as reported by other investigators;[21,34] and here its appearance is more pronounced at smaller pressure, contrary to the result of Kluson and Scaife.[34]

When we enlarge the viewing area of the small pore size, we can clearly see from Figure 10a for all pressures that the adsorbate density of CO_2 is oscillatory while the density of CH_4 keeps increasing as the pore become larger. It can be seen that at the first minimum at $H^* = 2.4$ (from Figure 9), the adsorbate density of CO_2 is also a minimum and gives the maximum density at $H^* = 2.7$ and 3.8. This first peak is likely due to the overlap of the potential walls, leading to strong adsorption of carbon dioxide molecules. As the peaks disappear when pores become larger (reduced pore width greater than 6) and the effect of confinement is reduced, a selectivity minimum followed by the second maximum are observed. This behavior is related to the oscillations in the capacity resulting from structural transitions between hexatic and square packing. Such oscillations have been studied in the literature and reported by other workers in this area.[27,35-37]

It is shown in Figures 11a and 11b (known as the X-Y diagram) that for the methane and carbon dioxide binary system, the adsorption of carbon dioxide is preferential on the studied slit-pore adsorbent model as mole fraction of carbon dioxide in the adsorbed phase is greater than in the bulk phase. The diagram presents the mole fraction of component 2 (herein carbon dioxide) in the gas phase (y_2) as a function of the mole fraction of component 2 in the adsorbed phase (x_2). It adsorbs more CO_2 at higher pressure as the affinity is increased with the

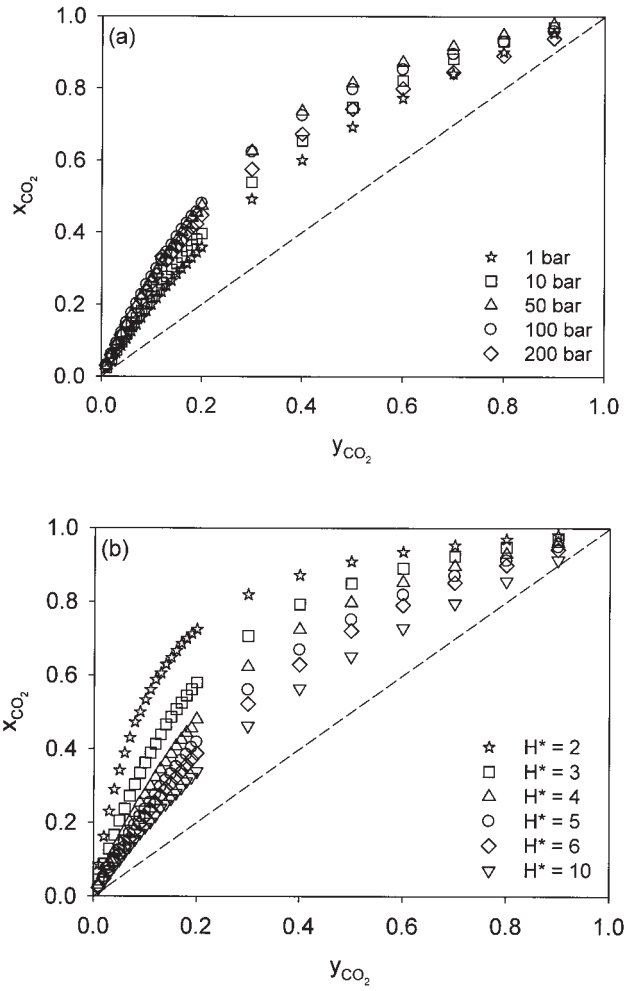

Figure 11. XY diagram for carbon dioxide at 318 K.

(a) Reduced slit-width (H^*) equal to 4, at various pressures, and (b) pressure 100 bar, at various reduced slit-widths.

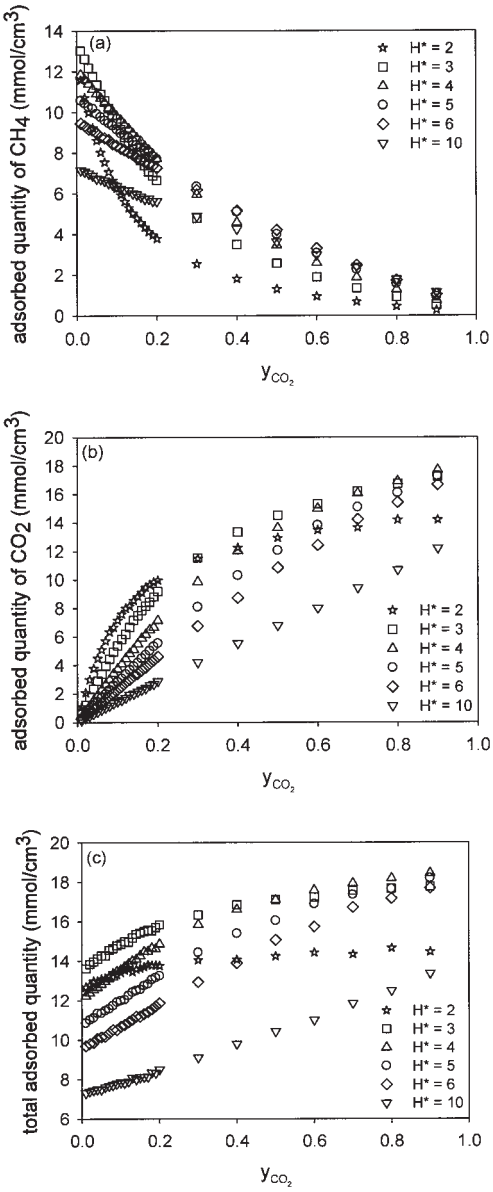

Figure 12. Adsorbed density of (a) methane, (b) carbon dioxide, and (c) total mixture, at temperature 318 K and pressure 100 bar for several reduced slit-widths.

pressure, and adsorbs more CO_2 at smaller pore size, as the interaction between the pore and the molecule is weaker with increase in the pore size. Also, all results are above the dashed diagonal line, which implies that the selectivity of CO_2 to CH_4 is larger than 1.

Simulated adsorption isotherms at 318 K and 100 bar, for several different pore sizes, for methane, carbon dioxide, and total mixture, are shown in Figures 12a, 12b, and 12c, respectively. At small CO_2 in the bulk, both methane and carbon dioxide are adsorbed more in smaller pores since they have stronger interaction, except for $H^* = 2$ in the case of methane. At this pore size, CO_2 is more easily adsorbed as it has stronger attraction with the wall and its molecular size is smaller than methane. When y_{CO_2} in the bulk is increased, the carbon dioxide displaces methane, and this effect is stronger in the smallest pore sizes because of the greater strength CO_2-carbon interaction in these pores. This is evident in Figure 12a, where the curves for the lower pore sizes show steeper declines in CH_4 adsorption. At the smallest pore size of $H^* = 2$, saturation is achieved at relatively low y_{CO_2}; and as Figure 12c shows, the binary adsorption is unchanged beyond about $y_{CO_2} = 0.2$.

Conclusions

Single and binary adsorption equilibria of methane and carbon dioxide in carbon slit-pores with different pore sizes for various temperatures and pressures have been studied, and results from the Denton-Ashcroft DFT and GCMC simulation have been compared. The latter shows the inadequacy of the DFT in describing the adsorption over a wide range of pressure.

Separation factors obtained are discussed as functions of the pressure, temperature, pore size, and bulk mole fraction of carbon dioxide. Adsorption of carbon dioxide is preferred to methane from binary mixtures under studied conditions. While the pressure is increased, the selectivity of carbon dioxide with respect to methane in the binary mixture initially increases to a maximum value at about the same pressure for every pore size and then decreases before becoming constant (i.e., independent of pressure). This optimum pressure is about 40 bar at 328 K, and is only weakly dependent on temperature. All selectivity results demonstrate that many factors can affect adsorptive separation for a gas mixture; therefore, optimization of the conditions is needed in practical CO_2 sequestration.

As small pore size has strong interaction potential energy between the adsorbate and the pore wall, higher selectivity is observed here. Varying the pressure will give different selectivity, while there is a much weaker selectivity variation with temperature. On increasing the mole fraction of CO_2 in the bulk, the selectivity goes through a maximum.

This present simulation knowledge on separation of carbon dioxide from a binary mixture of carbon dioxide and methane may constitute a good starting point for further research on carbon dioxide sequestration. Especially, promising is to treat other binary systems, such as carbon dioxide-nitrogen or nitrogen-methane, or even ternary mixtures.

Acknowledgments

The first author wishes to thank the Asian Development Bank through TPSDP-Loan No. 1792-INO for financial support in the form of a scholarship. We thank Thanh Nguyen for useful discussions.

Literature Cited

1. Houghton JT, Ding Y, Griggs DJ, Noguer M, van der Linden PJ, Dai X, Maskel K. *The Scientific Basis*. Cambridge: Cambridge University Press; 2001.
2. MaStalerz M, Glikson M. *Coalbed Methane: Scientific, Environmental and Economic Evaluation*. Dordrecht: Kluwer; 1999.
3. Yamasaki A. An overview of CO_2 mitigation options for global warming—emphasizing CO_2 sequestration options. *J Chem Eng Jpn.* 2003;36:361-375.
4. Cracknell RF, Gordon P, Gubbins KE. Influence of pore geometry on the design of microporous materials for methane storage. *J Phys Chem.* 1993;97:494-499.
5. Darkrim F, Vermesse J, Malbrunot P, Levesque D. Monte Carlo simulations of nitrogen and hydrogen physisorption at high pressures and room temperature. Comparison with experiments. *J Chem Phys.* 1999;110:4020-4027.

6. Gusev VY, O'Brien JA, Seaton NA. A self-consistent method for characterization of activated carbons using supercritical adsorption and grand canonical Monte Carlo simulations. *Langmuir.* 1997;13:2815-2821.
7. Heuchel M, Davies GM, Buss E, Seaton NA. Adsorption of carbon dioxide and methane and their mixtures on an activated carbon: simulation and experiment. *Langmuir.* 1999;15:8695-8705.
8. Jiang S, Zollweg JA, Gubbins KE. High-pressure adsorption of methane and ethane in activated carbon and carbon fibers. *J Phys Chem.* 1994;98:5709-5713.
9. Kaneko K, Shimizu K, Suzuki T. Intrapore field-dependent micropore filling of supercritical nitrogen in slit-shaped micropores. *J Chem Phys.* 1992;97:8705-8711.
10. Suzuki T, Kobori R, Kaneko K. Grand canonical Monte Carlo simulation-assisted pore-width determination of molecular sieve carbons by use of ambient temperature n2 adsorption. *Carbon.* 2000;38:630-633.
11. Tan Z, Gubbins KE. Adsorption in carbon micropores at supercritical temperatures. *J Phys Chem.* 1990;94:6061-6069.
12. Denton AR, Ashcroft NW. Weighted-density-functional theory of nonuniform fluid mixtures: application to the structure of binary hard-sphere mixtures near a hard wall. *Phys Rev A: At Mol Opt Phys.* 1991;44:8242-8248.
13. Bhatia SK. Adsorption of binary hydrocarbon mixtures in carbon slit pores. A density functional theory study. *Langmuir.* 1998;14:6231-6240.
14. Bhatia SK. Density functional theory analysis of the influence of pore wall heterogeneity on adsorption in carbons. *Langmuir.* 2002;18:6845-6856.
15. Weeks JD, Chandler D, Andersen HC. Role of repulsive forces in determining the equilibrium structure of simple liquids. *J Chem Phys.* 1971;54:5237-5247.
16. Allen MP, Tildesley DJ. *Computer Simulation of Liquids*. Oxford: Oxford University Press; 1987.
17. Norman GE, Filinov VS. Investigations of phase transitions by a Monte-Carlo method. *High Temp.* 1969;7:216.
18. Nicholson D, Parsonage NG. *Computer Simulation and the Statistical Mechanics of Adsorption*. New York: Academic Press; 1982.
19. Steele WA. Physical interaction of gases with crystalline solids. I. Gas-solid energies and properties of isolated adsorbed atoms. *Surf Sci.* 1973;36:317-352.
20. Cracknell RF, Nicholson D. Adsorption of gas mixtures on solid surfaces, theory and computer simulation. *Adsorption.* 1995;1:7-16.
21. Cracknell RF, Nicholson D, Tennison SR, Bromhead J. Adsorption and selectivity of carbon dioxide with methane and nitrogen in slit-shaped carbonaceous micropores: simulation and experiment. *Adsorption.* 1996;2:193-203.
22. Kaneko K, Cracknell RF, Nicholson D. Nitrogen adsorption in slit pores at ambient temperatures: comparison of simulation and experiment. *Langmuir.* 1994;10:4606-4609.
23. Lastoskie C, Gubbins KE, Quirke N. Pore size heterogeneity and the carbon slit pore: a density functional theory model. *Langmuir.* 1993;9:2693-2702.
24. Quirke N, Tennison SRR. The interpretation of pore size distributions of microporous carbons. *Carbon.* 1996;34:1281-1286.
25. Shigeta T, Yoneya J, Nitta T. Monte Carlo simulation study of adsorption characteristics in slit-like micropores under supercritical conditions. *Mol Simul.* 1996;16:291-305.
26. Sing KSW, Everett DH, Haul RAW, Moscou L, Pierotti RA, Rouquerol J, Siemieniewska T. Reporting physisorption data for gas/solid systems with special reference to the determination of surface area and porosity (recommendations 1984). *Pure Appl Chem.* 1985;57:603-619.
27. Bhatia SK, Tran K, Nguyen TX, Nicholson D. High-pressure adsorption capacity and structure of co2 in carbon slit pores: theory and simulation. *Langmuir.* 2004;20:9612-9620.
28. Nguyen TX, Bhatia SK, Nicholson D. Prediction of high-pressure adsorption equilibrium of supercritical gases using density functional theory. *Langmuir.* 2005;21:3187–3197.
29. Nicholson D. Simulation study of nitrogen adsorption in parallel-sided micropores with corrugated potential functions. *J Chem Soc, Faraday Trans.* 1994;90:181-185.
30. Bender E. Equations of state exactly representing the phase behavior of pure substances. *Proceedings of the Fifth Symposium On Thermophysical Properties.* 1970;1:227-235.
31. Span R, Wagner W. A new equation of state for carbon dioxide covering the fluid region from the triple-point temperature to 1100 k at pressures up to 800 mpa. *J Phys Chem Ref Data.* 1996;25:1509-1596.
32. Sandler SI. *Chemical and Engineering Thermodynamics*. New York: John Wiley & Sons; 1999.
33. Ruthven DM. *Principles of Adsorption and Adsorption Processes*. New York: John Wiley & Sons; 1984.
34. Kluson P, Scaife SJ. Microporous adsorbents for a selective separation of carbon dioxide from mixtures with methane and nitrogen. *Chem Biochem Eng Q.* 2002;16:97-103.
35. Nguyen TX, Bhatia SK, Nicholson D. Close packed transitions in slit-shaped pores: density functional theory study of methane adsorption capacity in carbon. *J Chem Phys.* 2002;117:10827-10836.
36. Nicholson D, Stubos T. Simulation of adsorption in micropores. *Membrane Science and Technology Series.* 2000;6:231-256.
37. Olivier JP. Improving the models used for calculating the size distribution of micropore volume of activated carbons from adsorption data. *Carbon.* 1998;36:1469-1472.

Manuscript received May 8, 2005, and revision received July 27, 2005.